except to a small extent through loss of power out of band. However, noise photons injected by the amplifiers and random photon deletion due to absorption cause the propagating field to acquire a stochastic component, which also leads to multiplicative noise effects through the nonlinear term. This leads us to believe that the single-user case will qualitatively exhibit the same decline in spectral efficiency with intensity as the multi-user case. The same qualitative arguments apply to interposing optical phase conjugation elements for nonlinear compensation; fibre absorption and amplifier noise can still be shown to cause multiplicative noise through the cubic term. It would be incorrect to conclude that nonlinearities must always impair capacity: signal regenerators are an obvious conter-example. However, the fundamental insight in the current work is that in nonlinear propagation channels, qualitatively new phenomena that arise from multiplicative noise effects can severely degrade capacity. □

Methods

Gaussian bound to the channel capacity

Proof of the inequality $I(X_G, Y) \geqslant I(X_G, Y_G)$: define $p(X, Y)$ as the product $p_G(X)p(Y|X)$, and $p_G(X, Y)$ to be the joint gaussian distribution having the same second moments as $p(X, Y)$. Also define $p_G(Y)$ to be the corresponding marginal of $p_G(X, Y)$.

$$I(X_G, Y) = \int dX dY p(X, Y) \log\left(\frac{p(X, Y)}{p_G(X)p(Y)}\right) \quad (4)$$

$$= \int dX dY p(X, Y)\left[\log\left(\frac{p_G(X, Y)}{p_G(X)p_G(Y)}\right) - \log\left(\frac{p_G(X, Y)p_G(Y)}{p(X, Y)p_G(X)}\right)\right] \quad (5)$$

As $p(X, Y)$ and $p_G(X, Y)$ share second moments, the first term on the right-hand side is $I(X_G, Y_G)$. The second term may be simplified using the convexity of the logarithm, $\langle\log(f)\rangle \leqslant \log(\langle f\rangle)$ to obtain

$$I(X_G, Y) \geqslant I(X_G, Y_G) - \log\left[\int dX dY p_G(X, Y)\frac{p(Y)}{p_G(Y)}\right] \quad (6)$$

$$\geqslant I(X_G, Y_G). \quad (7)$$

The second inequality follows by first performing the integral over X, and noting that $\log(\int dY p(Y)) = \log(1) = 0$.

Derivation of the average propagator $\langle U\rangle$

This can be done by resumming the perturbation series exactly for $\langle U\rangle$, for delta-correlated $V(z, t)$. Alternatively, using path integrals[7], $\langle U(t, t'; L)\rangle = U_0(t - t'; L)\langle\langle\exp(i\int_0^L dz V(z, t(z)))\rangle\rangle$, where the average is taken over V as well as over paths $t(z)$ satisfying $t(0) = t$, $t(L) = t'$. The result in the text follows by performing the gaussian average over V. Because $\phi = \int_0^L dz V(z, t(z))$ is a linear combination of gaussian variables, it is also gaussian-distributed and satisfies $\langle\exp(i\phi)\rangle = \exp(-\langle\phi^2\rangle/2)$. The result follows by noting that for delta-correlated V, $\langle\phi^2\rangle$ is a constant given by ηL. The delta correlations need to be treated carefully; this can be done by smearing the delta functions slightly and leads to the definition of η given earlier in the text.

Received 13 November 2000; accepted 19 April 2001.

1. Shannon, C. E. A mathematical theory of communications. *Bell Syst. Tech. J.* **27,** 379–423, 623–656 (1948).
2. Biglieri, E., Proakis, J. & Shamai, S. Fading channels: Information-theoretic and communications aspects. *Inform. Theory Trans.* **44,** 2619–2692 (1998).
3. Kogelnik, H. High-capacity optical communication. *IEEE Sel. Topics Quant. Elec.* **6**(6), 1279 (2000).
4. Agrawal, G. P. *Nonlinear Fiber Optics* (Academic, San Diego, 1995).
5. Desurvire, E. *Erbium Doped Fibre Amplifiers* 69 (Wiley, New York, 1994).
6. Cover, T. M. & Thomas, J. A. *Information Theory* 374–458 (Wiley, New York, 1991).
7. Feynman, R. P. & Hibbs, R. A. *Quantum Mechanics and Path Integrals* (McGraw-Hill, New York, 1963).

Acknowledgements

We gratefully acknowledge extensive discussions with E. Telatar, and also with A. Green, P. B. Littlewood, R. Slusher, A. Chraplyvy and G. Foschini. We thank M. Povinelli and L. Wegener for performing numerical and analytical computations to verify the considerations in this Letter, and D. R. Hamann and R. Slusher for careful readings of the manuscript.

Correspondence and requests for materials should be addressed to P.P.M. (e-mail: pmitra@bell-labs.com).

Control of conformational and interpolymer effects in conjugated polymers

J. Kim*† **& T. M. Swager**‡†

* *Department of Materials Science and Engineering,* † *Center for Materials Science and Engineering, and* ‡ *Department of Chemistry, Massachusetts Institute of Technology, Cambridge, Massachusetts 02139, USA*

The role of conjugated polymers in emerging electronic, sensor and display technologies is rapidly expanding. In spite of extensive investigations[1–11], the intrinsic spectroscopic properties of conjugated polymers in precise conformational and spatial arrangements have remained elusive. The difficulties of obtaining such information are endemic to polymers, which often resist assembly into single crystals or organized structures owing to entropic and polydispersity considerations. Here we show that the conformation of individual polymers and interpolymer interactions in conjugated polymers can be controlled through the use of designed surfactant poly(*p*-phenylene-ethynylene) Langmuir films. We show that by mechanically inducing reversible conformational changes of these Langmuir monolayers, we can obtain the precise interrelationship of the intrinsic optical properties of a conjugated polymer and a single chain's conformation and/or interpolymer interactions. This method for controlling the structure of conjugated polymers and establishing their intrinsic spectroscopic properties should permit a more comprehensive understanding of fluorescent conjugated materials.

We designed and synthesized (see Supplementary Information for details) four poly(*p*-phenylene-ethynylene) compounds (PPEs) using four surfactant 'building blocks' that display preferential orientations at the air–water interface. Unique combinations of these building blocks (A–D in Fig. 1) allow us to control an isolated polymer chain's conformation and interpolymer interactions. Building block A, with two *para*-hydrophobic dioctylamide groups, is expected to display a face-on structure, with its phenyl groups co-facial to the air–water interface[12,13]. B has two *para*-hydrophilic triethyleneoxide groups, and is also expected to prefer a face-on structure. The third building block, C, has one hydrophobic and one hydrophilic group *para* to each other, and is inclined towards an equilibrium edge-on structure with the π-plane normal to the interface. The last block, D, with two *ortho*-hydrophobic dodecyloxy groups, favours an edge-on structure. By design we have used these four building blocks to produce PPEs with precise structural features at the air–water interface. As we will show below, these polymers display one of three equilibrium organizations—face-on, alternating face-on and edge-on (zipper), or edge-on—depending upon the structure and surface pressure (Fig. 1).

Central to our analysis is the ability to switch between different structures, by applying mechanical force while monitoring the Langmuir monolayer's optical spectra. Figure 1 shows the chemical structures, conformations and spatial arrangements at the air–water interface of the PPEs. Our assignments of the conformations and spatial arrangements are based on a self-consistent analysis of the pressure–area (P–A) isotherms (Fig. 2a), *in situ* ultraviolet–visible (UV–vis.) and fluorescence spectroscopy (Fig. 3), and molecular modelling (Fig. 2b). Polymer **1** favours the face-on structure with a large extrapolated area per repeating unit of 240 Å^2. As the monolayer is compressed, the surface pressure increases until the monolayer folds into multilayers at 30 mN m^{-1} with an area per repeating unit of 130 Å^2. Molecular modelling predicts a repeating unit area of 126 Å^2 when **1** is highly compressed in the face-on structure (Fig. 2b). The wavelength of maximum

absorption (λ_{max}) of **1** at the air–water interface at 0 mN m^{-1} is red-shifted by 35 nm relative to its solution value owing to the increased π-conjugation length in the face-on structure[5,14]. Our studies point to the polymer having a highly non-planar structure in solution (see below). Compression perturbs the π-conjugation system, causing the blue shift in absorption spectra with increased pressure (Fig. 3a). During the compression, the fluorescence quantum yield is unchanged, indicating—as expected—that edge-to-edge interpolymer interactions do not affect the quantum yield (Fig. 3b). After the monolayer of **1** folds into a multilayer at 30 mN m^{-1}, aggregated fibrils are visually observed. *In situ* UV–vis. spectroscopy also shows an additional aggregation peak at 464 nm, 13 nm to the red of the absorption λ_{max} of the face-on structure with the maximized π-conjugation. We confirmed that the 464-nm band is the result of interpolymer co-facial π–π interactions by conducting the same *in situ* UV–vis. experiment on a previously studied polymer[15] that is isostructural except that the ethylene oxide side chains of B are part of a macrocycle that prevents strong interchain electronic interactions. In this case, even after the folding into a multilayer, the UV–vis. spectrum does not show the aggregation peak at 464 nm. We note that the polymer conformation in the aggregated state probably exhibits an extended conjugation, which will facilitate the strong interpolymer electronic interactions. The P–A isotherm of **1** is completely reversible, as are the spectroscopic changes.

Polymer **2** also shows completely reversible P–A isotherms and spectroscopic changes during cycles. The extrapolated area per repeating unit of 240 Å^2 for **2** is the same as for **1**, confirming the face-on structure. A distinct difference of the P–A isotherm of **2** is the transition between 15 and 20 mN m^{-1}, when the orientation of the C repeating units change to an edge-on structure, allowing further compression up to 90 Å^2. We refer to **2**'s new alternating face-on and edge-on conformation (with neighbouring chains interlocked) as a zipper structure (Fig. 1). The areas per repeating unit predicted by molecular modelling are 196 Å^2 and 134 Å^2 for the face-on and the zipper structure respectively, which are in good agreement with the P–A isotherm (Fig. 2). The transition point (140 Å^2) in the P–A isotherm was calculated from the second derivative of the isotherm.

The spectroscopic measurements also support this zipper structure. Initial compression up to 15 mN m^{-1} causes the same minor perturbation of the π-conjugation system as in the case of **1**. However, continued compression from 15 to 20 mN m^{-1} causes a transition from the face-on to the zipper structure, which decreases the π-conjugation length thereby generating a large (21-nm) blue shift. A 34-nm blue shift is observed over the entire compression (0–20 mN m^{-1}). The fluorescence spectrum also showed a 9-nm blue shift with the face-on to zipper transition. The 38% increase in quantum yield is probably due to a larger energy gap and reduced intramolecular dynamics in the compressed state. The larger energy separation of the lowest singlet excited state, S_1, and the ground state S_0, decreases the Franck–Condon overlaps of the nuclear wavefunctions that control the internal conversion rate, and therefore an improved quantum yield is expected[16]. It is also possible that an interlocked zipper structure, which lacks extended π-conjugation, reduces the exciton's diffusion length thereby reducing quenching with molecular oxygen or other impurities. The λ_{max} of the initial face-on structure is red-shifted by 38 nm relative to solution,

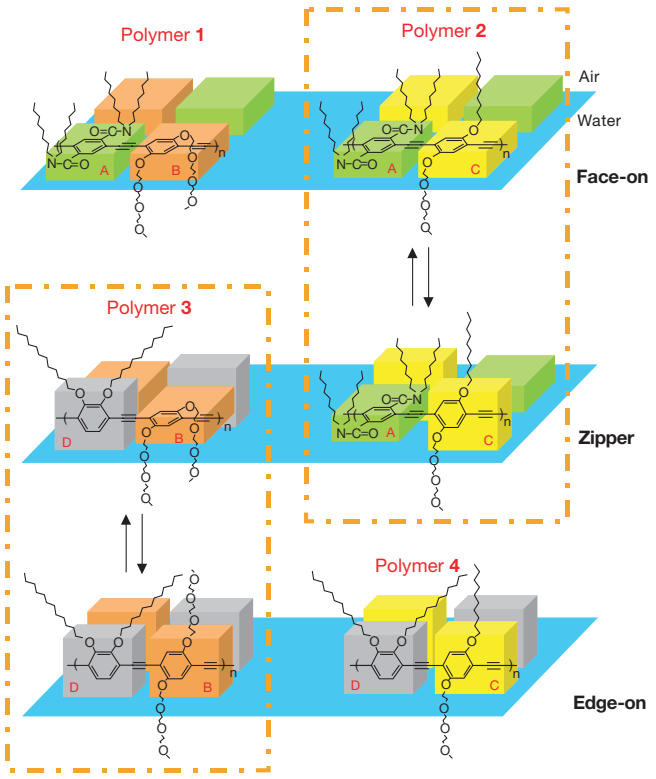

Figure 1 Conformations and spatial arrangements of polymers **1**–**4** at the air–water interface and their reversible conversions between face-on, zipper and edge-on structures. Polymer **1**: number-average molecular mass M_n = 23,000, Poly-dispersity index, PDI = 2.4. Polymer **2**: M_n = 293,000, PDI = 1.7. Polymer **3**: M_n = 115,000, PDI = 2.2. Polymer **4**: M_n = 96,000, PDI = 2.8. The monomers A, B, C and D are represented by green, orange, yellow and grey boxes, respectively.

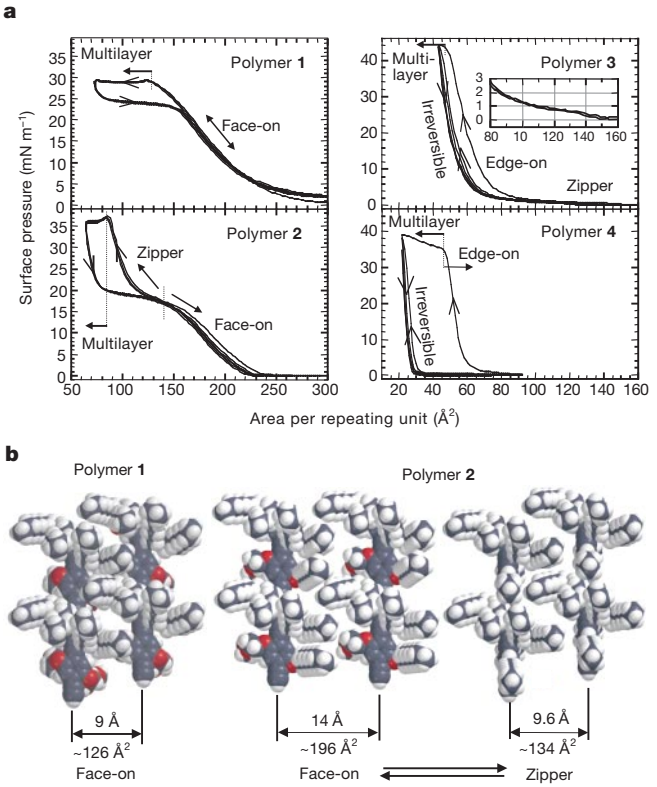

Figure 2 Pressure–area (P–A) isotherms of polymers **1**–**4** and projected areas from molecular models. **a**, P–A isotherms. **b**, Molecular models of adjacent polymer packing. Top views of two repeating units of polymers **1** and **2** are shown. The calculated length of one repeating unit is 14 Å, which is used to calculate the area per repeating unit from the modelling.

indicating, as mentioned earlier, that a non-planar conformation similar to the zipper structure is present in solution. The blue-shifted fluorescence λ_{max} of the zipper phase (462 nm) is also similar to the solution value (457 nm). The zipper structure is further supported by the synthesis of polymers with small amounts of ethynylene homo-coupling (that is, diacetylene groups) that disrupt the interlocking structure of polymer chains. A regularly alternating -A-C-A-C-A-C- structure is required to observe clear transitions in the P–A isotherm. Small amounts of an -A-C-C-A-C- imperfection[17] gives a less-featured P–A isotherm. After a monolayer of **2** folds into a multilayer film, a similar behaviour to that of **1** is observed, with the formation of an aggregation peak at 470 nm.

Langmuir monolayers of polymer **3** appear to assemble into the zipper structure before compression, and have an extrapolated area per repeating unit of 150 Å^2 that is much smaller than that of **1** and **2**. This zipper structure is promoted by the phenyl ring of building block D, which, when orientated normal to the surface, minimizes contact between the two hydrophobic sidechains and the water. The shape and λ_{max} of **3**'s uncompressed monolayer absorption and fluorescence spectra are consistently the same as those in solution. As **3** is compressed, one of the moderately hydrophilic triethylene-oxide groups from building block B is removed from the aqueous phase, and the film transforms from a zipper to an edge-on structure between 150 and 100 Å^2. This structural transition is probably facilitated by favourable interpolymer dipolar interactions between these polar side chains in the edge-on structure.

In the edge-on structure polymer **3** is co-facially arranged, and—as we have previously established—π-aggregation between main chains generates a new aggregation band in the UV–vis (Fig. 3a) spectra. This new narrow red-shifted band with a distinct shoulder is characteristic of a π-aggregated state with lower quantum yields, and should be distinguished from the red-shift owing to planarization alone[18] observed for **1** and **2**. The film in an edge-on structure is aggregated before film collapse; therefore no new band arises upon folding into a multilayer. As the aggregation band in the UV–vis. spectra grows the fluorescence is quenched, and when completely aggregated the quantum yield drops to 16% of the initial non-aggregated value (Fig. 3b). Before the folding of the monolayer into multilayers, the transition from the zipper to the edge-on structure is completely reversible. Therefore, releasing the surface pressure de-aggregates the film, and the initial absorbance and fluorescence spectra are re-established.

Polymer **4** has two edge-on building blocks, and forms the edge-on structure even before compression. Molecular modelling for **3** and **4** in an edge-on structure predicts an area per repeating unit of 64 Å^2, which is consistent with the value of 60 Å^2 from the P–A isotherm. As the film is compressed, the fluorescence intensity gradually decreases because the reduced distance between co-facially arranged polymer main chains promotes self-quenching[19,20]. The area per repeating unit at which the monolayer folds into

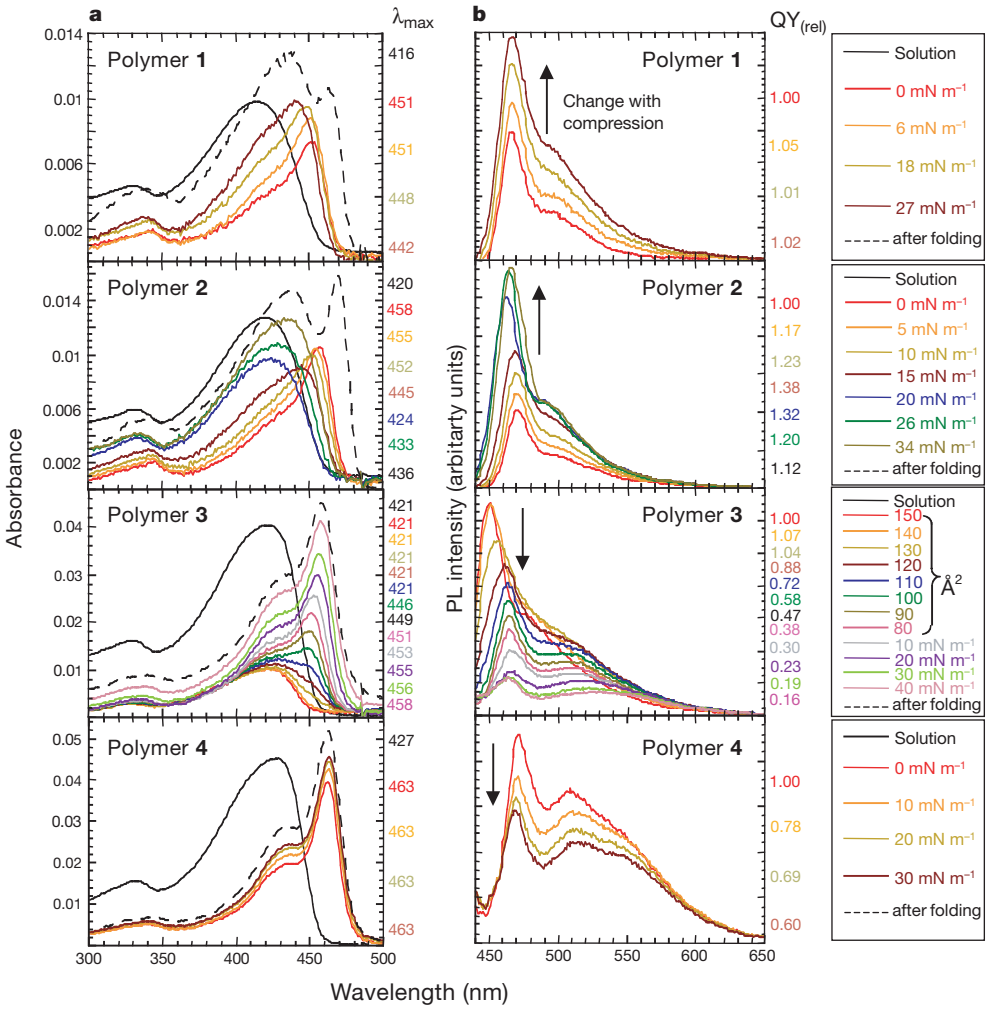

Figure 3 *In situ* UV–vis. and fluorescence spectra of Langmuir monolayers of polymers **1**–**4** during cycles of compressions and expansions. Polymer solutions were prepared in chloroform. **a**, *In situ* UV–vis. spectra and λ_{max} at various surface pressures. **b**, *In situ* fluorescence spectra and relative quantum yields (QY_{rel}) at various surface pressures and area per repeating units (relative quantum yield at 0 mN m^{-1} = 1). Excitation wavelength was 420 nm.

multilayers is 50 Å^2, the same value as for polymer **3**. This observation also supports the transition of **3** from the zipper to the edge-on. The aggregate emission bands are also identical with those of highly compressed **3**. The aggregate features are present at an area per repeating unit of 60 Å^2. This value and a repeat unit length of 14 Å provide an interpolymer distance of 4.3 Å, provided that the phenyl rings are standing perpendicular to the air–water interface. At higher pressures the emission is further quenched, and at the maximum compression of monolayers of polymers **3** and **4** the area per repeating unit is 50 Å^2, which provides an interpolymer spacing of 3.6 Å. The red-shifted absorption band implies that the aggregation is probably J-type. But because we have no knowledge of the registry of polymer chains with respect to each other, we cannot confirm whether the aggregation is of type H (in phase) or type J (out of phase).

To verify the nature of the emission peak at 471 nm and the sharp absorption peak at 463 nm for polymer **4**, we conducted non-solvent induced aggregation studies. Polymer **4** was dissolved in chloroform, and then UV–vis. and fluorescence spectra were taken as methanol, a non-solvent, was gradually added to the solution. Above equal amounts of chloroform and methanol, the polymer aggregates and absorption spectra display a pseudo-isosbestic point. (An isosbestic point implies that there are two different interconverting species.) Because of the limited solubility of **4**, it was technically difficult to conduct the experiment at a constant molar concentration, which is a necessary condition for a true isosbestic point. The absorption λ_{max} of the aggregate is 460 nm, close to the 463 nm of **4** at the air–water interface. The non-aggregated emission peak at 452 nm is continuously suppressed with added methanol until the spectrum has a main peak at 475 nm and two other peaks at about 510 and 545 nm. The final fluorescence spectrum is almost identical with the fluorescence spectrum of **4** in the edge-on structure at the air–water interface.

Excitation spectra of a solution in which an aggregated and a non-aggregated phase coexist have been collected by monitoring the emissions at 450, 475, 510 and 545 nm. The emission peak at 450 nm corresponds to the non-aggregated phase, as its excitation spectrum displays a maximum at 420 nm. The emission peaks at 475, 510 and 545 nm all have the same excitation spectra with peaks at 420 and 460 nm. Therefore, these three peaks are the result of polymer aggregates. The presence of the 420-nm peak in the excitation spectra is due to energy transfer from the higher-energy non-aggregated phase to the aggregated phase. We can discount the possibility of an excimer because we clearly see a ground-state absorption that is responsible for the new emission bands[21]. An excimer is an excited state complex, and should not result in new absorption bands. The lifetime of the non-aggregated band at 450 nm is 0.5 ns, and those of the other bands at 475, 510 and 545 nm are 0.1–0.2 ns. The lifetimes of excimers are often much longer than intrachain excitons[21], which also supports the fact that the longer-wavelength bands are not excimer peaks.

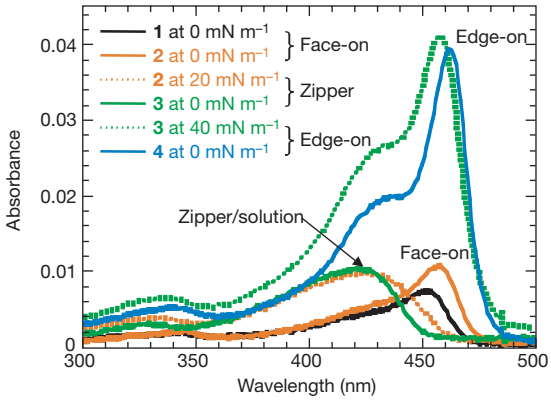

Figure 4 Selected UV–vis. spectra of polymers **1**–**4** in different structures (face-on, zipper, and edge-on). These data show the interrelationship between the conformation and interpolymer interactions.

Selected UV–vis. spectra of **1**–**4** from Fig. 3a are compared in Fig. 4. These spectra show the self-consistency of our results that have allowed us to unambiguously assign the structures to different spectral attributes. Polymers **1** and **2** have the same face-on structure at 0 mN m^{-1}; then mechanical pressure at 20 mN m^{-1} induces transition of **2** into the zipper structure—which **3** has initially at 0 mN m^{-1}. Mechanical compression of **3** causes the transition into the edge-on structure with a co-facial π-aggregation band that **4** has at 0 mN m^{-1}.

The combination of unique surfactant design and mechanical interrogation at the air–water interface have allowed us to show the interrelationships between the conformation of a single chain and the interpolymer interactions and a conjugated polymer's absorption and emission properties. Although these materials have been studied extensively[1–4,8,10–11,14], the intrinsic properties of isolated chains and ordered aggregates have yet to be established. The influence of structure on the charge- and energy-transporting properties of conjugated polymers could also be addressed by extensions of the methods presented here. □

Methods

A Nima 601 M model Langmuir–Blodgett trough with a window was used for the studies. The *in situ* UV–vis. spectra were obtained on a Hewlett-Packard 8453 diode array spectrophotometer or a Cary 50 Scan with fibre optics. The *in situ* fluorescence studies were conducted with a SPEX Fluorolog-τ2 fluorometer equipped with fibre optics. All the spectroscopic measurements on Langmuir films were conducted through optical fibres. Molecular modelling was performed using the Spartan 5.0 molecular modelling program (Wavefunction Inc, Irvine, California) running on a SGI O2 (R12000) workstation. These calculations are intended to give good estimates of the areas per repeating unit and required some geometric constraints that simulate the organizational preferences at the air–water interface.

Received 8 February; accepted 13 April 2001.

1. Nguyen, T.-Q., Wu, J., Doan V., Schwartz, B. J. & Tolbert, S. H. Control of energy transfer in oriented conjugated polymer-mesoporous silica composites. *Science* **288,** 652–656 (2000).
2. Shi, Y., Liu, J. & Yang, Y. Device performance and polymer morphology in polymer light emitting diodes: The control of thin film morphology and device quantum efficiency. *J. Appl. Phys.* **87,** 4254–4263 (2000).
3. Nguyen, T.-Q., Martini, I. B., Liu, J. & Schwartz, B. J. Controlling interchain interactions in conjugated polymers: The effects of chain morphology on exciton-exciton annihilation and aggregation in MEH-PPV films. *J. Phys. Chem. B* **104,** 237–255 (2000).
4. Sirringhaus, H. *et al.* Two-dimensional charge transport in self-organized, high-mobility conjugated polymers. *Nature* **401,** 685–688 (1999).
5. Lucht, B. L., Mao, S. S. H. & Tilley, T. D. A zirconocene-coupling route to substituted poly(*p*-phenylenedienylene)s: Band gap tuning via conformational control. *J. Am. Chem. Soc.* **120,** 4354–4365 (1998).
6. Cornil, J., dos Santos, D. A., Crispin, X., Silbey, R. & Brédas, J. L. Influence of interchain interactions on the absorption and luminescence of conjugated oligomers and polymers: A quantum-chemical characterization. *J. Am. Chem. Soc.* **120,** 1289–1299 (1998).
7. Yang, J.-S. & Swager, T. M. Fluorescent porous polymer films as TNT chemosensors: Electronic and structural effects. *J. Am. Chem. Soc.* **120,** 11864–11873 (1998).
8. Buvat, P. & Hourquebie, P. Enhanced infrared properties of regioregular poly(3-alkylthiophenes). *Macromolecules* **30,** 2685–2692 (1997).
9. Jenekhe, S. A. & Osaheni, J. A. Excimers and exciplexes of conjugated polymers. *Science* **265,** 765–768 (1994).
10. Gettinger, C. L., Heeger, A. J., Drake, J. M. & Pine, D. J. A photoluminescence study of poly(phenylene vinylene) derivatives—The effect of intrinsic persistence length. *J. Chem. Phys.* **101,** 1673–1678 (1994).
11. Heun, S. *et al.* Conformational effects in poly(*p*-phenylene vinylene)s revealed by low-temperature site-selective fluorescence. *J. Phys. Condens. Matter* **5,** 247–260 (1993).
12. Kim, J., McHugh, S. K. & Swager, T. M. Nanoscale fibrils and grids: Aggregated structures from rigid-rod conjugated polymers. *Macromolecules* **32,** 1500–1507 (1999).
13. Josefowicz, J. Y. *et al.* Structure of Langmuir-Blodgett films of disk-shaped molecules determined by atomic force microscopy. *Science* **260,** 323–326 (1993).
14. Zhang, Q. T. & Tour, J. M. Imine-bridged planar poly(phenylenethiophene)s and polythiophenes. *J. Am. Chem. Soc.* **119,** 9624–9631 (1997).
15. Levitsky, I. A., Kim, J. & Swager, T. M. Energy migration in a poly(phenylene ethynylene): determination of interpolymer transport in anisotropic Langmuir-Blodgett films. *J. Am. Chem. Soc.* **121,** 1466–1472 (1999).
16. Turro, N. J. *Modern Molecular Photochemistry* 183 (University Science Books, Sausalito, California, 1991).
17. Kloppenburg, L., Jones, D. & Bunz, U. H. F. High molecular weight poly(p-phenyleneethynylene)s by alkyne metathesis utilizing "instant" catalysts: A synthetic study. *Macromolecules* **32,** 4194–4203 (1999).

18. Miteva, T., Palmer, L., Kloppenburg, L., Neher, D. & Bunz, U. H. F. Interplay of thermochromicity and liquid crystalline behavior in poly(*p*-phenyleneethynylene)s: π-π interactions or planarization of the conjugated backbone? *Macromolecules* **33,** 652–654 (2000).
19. McQuade, D. T., Kim, J. & Swager, T. M. Two-dimensional conjugated polymer assemblies: Interchain spacing for control of photophysics. *J. Am. Chem. Soc.* **122,** 5885–5886 (2000).
20. Kim, J., McQuade, D. T., McHugh, S. K. & Swager, T. M. Ion-specific aggregation in conjugated polymers: Highly sensitive and selective fluorescent ion chemosensors. *Angew. Chem. Int. Edn Engl.* **39,** 3868–3872 (2000).
21. Cronwell, E. Excimer formation and luminescence in conducting polymers. *Trends Polym. Sci.* **5,** 218–222 (1997).

Supplementary information is available on *Nature*'s World-Wide Web site (http://www.nature.com) or as paper copy from the London editorial office of *Nature*.

Acknowledgements

We thank Z. Zhu for providing 1,2-didodecyloxy-3,6-diethynylbenzene (building block D), and A. Rose for the lifetime measurements. This work was supported by the Office of Naval Research and Draper Laboratory.

Correspondence and requests for materials should be addressed to T.M.S. (e-mail: tswager@mit.edu).

Biodegradation of oil in uplifted basins prevented by deep-burial sterilization

A. Wilhelms*, S. R. Larter†, I. Head†, P. Farrimond†, R. di-Primio* & C. Zwach*

* *Norsk Hydro Research Centre, PO 7190, 5020 Bergen, Norway*
† *Fossil Fuels and Environmental Geochemistry Postgraduate Institute (NRG), University of Newcastle, Newcastle upon Tyne NE1 7RU, UK*

Biodegradation of crude oil by bacterial activity—which has occurred in the majority of the Earth's oil reserves[1]—is known to reduce greatly the quality of petroleum in reservoirs[2]. For economically successful prospecting for oil, it is therefore important to understand the processes and conditions in geological formations that lead to oil biodegradation. Although recent studies speculate that bacterial activity can potentially occur up to temperatures as high as 150 °C (refs 3, 4), it is generally accepted that effective petroleum biodegradation over geological timescales generally occurs in reservoirs with temperatures below 80 °C (ref. 2). This appears, however, to be at odds with the observation that non-degraded oils can still be found in reservoirs below this temperature. Here we compile data regarding the extent of oil biodegradation in several oil reservoirs, and find that the extensive occurrence of non-biodegraded oil in shallow, cool basins is restricted to those that have been uplifted from deeper, hotter regions of the Earth. We suggest that these petroleum reservoirs were sterilized by heating to a temperature around 80–90 °C during deep burial, inactivating hydrocarbon-degrading organisms that occur in the deep biosphere. Even when such reservoirs are subsequently uplifted to much cooler regions and filled with oil, degradation does not occur, implying that the sterilized sediments are not recolonized by hydrocarbon-degrading bacteria.

Biodegradation of oil leads to a systematic decrease in paraffin content and an increase in oil density, sulphur content, acidity and viscosity[2], with negative economic consequences for oil production and refining operations. So prediction of the degree of biodegradation of oil is important for assessing the risk of finding degraded oils in an exploration target before drilling. The details and rates of the processes involved in crude-oil degradation are still poorly understood, but the central role of bacteria in subsurface petroleum degradation is accepted. Although there is abundant evidence for the presence of active bacteria deep (>1 km) in the Earth's crust[3,5–7], and a view among biologists that life in deep sediments may occur even up to 150 °C (refs 3, 4), there is a general view today among petroleum geoscientists that biodegradation in reservoirs ceases around 75–80 °C (refs 2, 8) in the zone of thermophilic organisms.

Hyperthermophilic organisms grow best above 80 °C, and have been reported to live at temperatures of up to 113 °C (ref. 9), but often display no growth below 60 °C (ref. 4). Most reports of hyperthermophilic activity are limited to environments rich in reduced electron donors, electron acceptors and inorganic nutrients necessary for biosynthesis—environments typically associated with shallow sediment or near-surface hydrothermal activity[10], where high levels of metabolic activity can be supported. Although petroleum reservoirs are rich in reduced organic electron donors (hydrocarbons), most petroleum reservoirs and deep aquifers are nutrient depleted[11] and recent studies indicate that biodegradation of petroleum in deep reservoirs is occurring at very slow net rates, typically consuming around 10^{-6} mmol oil per litre per day (ref. 12). These are similar to the respiration rates suggested for other deep sediments, and several orders of magnitude slower than respiration rates in anaerobic laboratory or near-surface sediment environments[11,13,14]. As electron donor (oil) supply is not limiting, degradation is presumably nutrient limited. Under these stressed, nutrient-limited conditions, it is unlikely that the temperature extremes survived by organisms in nutrient-rich hydrothermal environments are relevant. Furthermore, the empirical upper temperature limit of 80 °C observed for petroleum biodegradation in deep reservoirs is considerably lower than temperatures quoted for the denaturation and decomposition of many bacterial and archaeal proteins and nucleic acids[9,15]; this implies that active hyperthermophilic hydrocarbon-degraders are probably not present in petroleum reservoirs. Indeed, the single report of a hyperthermophilic archaeon that grew in enrichment cultures with crude oil as sole source of carbon[16] did not provide unequivocal evidence that the hyperthermophiles isolated could degrade hydrocarbons.

Although the occurrence of hyperthermophiles in petroleum reservoirs is now well documented[17–21], only four isolates capable of growth at greater than 90 °C have been reported[16–19]. In the most extreme of these cases (growth at 102 °C), evidence was presented that suggested that the organisms concerned may have originated from hydrothermal vent systems and were introduced with injected sea water[16]. The other cases where hyperthermophiles have been isolated are also sea-water-flooded reservoirs[19]. For the most part, microbial enrichments from petroleum reservoir samples conducted at temperatures above 85 °C have been unsuccessful[19,21], with increasing success of enrichment cultures with decreasing growth temperature (reaching 77% ($n = 26$) at temperatures below 60 °C)[19]. We also note that the only thermophilic anaerobic bacterium for which hydrocarbon degradation has been unequivocally demonstrated (an anaerobic sulphate-reducer) has an optimum growth temperature of only 60 °C (ref. 22). It has also been found that enrichment cultures supplied with crude oil as the sole source of organic carbon at temperatures greater than 85 °C failed to produce cultures of putative hydrocarbon-degrading Archaea although hyperthermophiles that grow at temperatures up to 102 °C could be isolated[16]. Taken together, data from most reports of Bacteria and Archaea isolated from petroleum reservoirs support the notion that the organisms which inhabit these reservoirs do not thrive in the upper temperature ranges for hyperthermophiles (up to 113 °C), and show little indication of hydrocarbon degrading capacity above 80 °C. We realize, however, that any interpretation must be viewed cautiously (as most reports provide little information on failed enrichments, and recent experience in defining the limits of life warn of inherent difficulty in definitively excluding life processes from even severe environments).

Biodegraded oils are common in cool (<80 °C), shallow reservoirs in currently subsiding basins such as those in the North Sea,